Transient-State Kinetic Analysis of the Oxidative Decarboxylation of D-Malate Catalyzed by Tartrate Dehydrogenase†

Peter A. Tipton*

Department of Biochemistry, University of Missouri—Columbia, Columbia, Missouri 65211

Received August 8, 1995; Revised Manuscript Received January 3, 1996⊗

ABSTRACT: The oxidative decarboxylation of D-malate catalyzed by tartrate dehydrogenase has been analyzed by transient-state kinetic methods and kinetic isotope effect measurements. The reaction time courses show a burst of NADH formation prior to the attainment of the steady-state velocity. The binding of the inhibitor tartronate to the enzyme was examined by monitoring the quenching of the protein's intrinsic fluorescence; the tartronate concentration dependence of the observed rate constant for association was hyperbolic, supporting a two-step model for inhibitor binding. Analysis of the time courses for D-malate oxidation yielded values for many of the microscopic rate constants governing the reaction. The range of possible solutions for the microscopic rate constants was constrained by comparison of the time course for oxidation of unlabeled malate with that of deuterated malate; this analysis relied on the determination of the intrinsic isotope effect on hydride transfer via measurement of $^{D}(V/K)$, $^{T}(V/K)$, and the oxaloacetate partition ratio. The results of the transient-state kinetic analyses suggest that the rate of D-malate oxidation is largely limited by the rate of decarboxylation of the intermediate oxaloacetate which occurs at 11 s^{-1}. Hydride transfer from D-malate to NAD^+ occurs with a rate constant of 300 s^{-1}, and ^{D}k for this step is 5.5. The agreement between experimentally measured steady-state kinetic parameters and kinetic isotope effects and their values calculated from the microscopic rate constants derived from the transient-state kinetic analyses was quite good.

Tartrate dehydrogenase is an NAD-dependent enzyme which exhibits a multiplicity of catalytic activities at a single active site (Tipton & Peisach, 1990). These activities appear to arise from the enzyme's ability to catalyze a branched reaction pathway in which the various substrates undergo the same initial catalytic steps but dissociate from the active site at different stages of the catalytic cycle, leading to different products. The three archetypal substrates are (+)-tartrate, D-malate, and *meso*-tartrate, which yield oxaloglycolate, pyruvate, and D-glycerate, respectively. These products arise from reaction sequences in which the substrate is oxidized [(+)-tartrate], oxidized and decarboxylated (D-malate), and oxidized, decarboxylated, and reduced (*meso*-tartrate).

According to the branched pathway model, the fate of a given substrate is determined by the height of the energy barriers surrounding the intermediates along the catalytic pathway. The product is formed, by definition, when the energy barrier for release of the species bound at the active site is lower than the energy barrier for further chemical transformation of that species. Because the three substrates and the intermediates which arise from them are so similar, TDH[1] is an ideal system in which to examine how enzymes exert control over the inherent chemical reactivities of their substrates.

We have applied transient-state kinetic studies and kinetic isotope effect measurements to derive an internally consistent kinetic description of the TDH-catalyzed oxidative decarboxylation of D-malate. These data allow aspects of the model described above to be put on a more quantitative footing.

MATERIALS AND METHODS

TDH was isolated from *Escherichia coli* cells carrying the plasmid pTDH1, which expresses the gene encoding TDH at high levels (Tipton & Beecher, 1994). The purification of the enzyme was accomplished as described before (Tipton & Peisach, 1991). The transient-state kinetic measurements were conducted using a preparation of TDH which had a specific activity of 0.6 U/mg. The concentration of TDH in each experiment was determined from absorbance measurements using a value for ϵ_{280} of 61 360 M^{-1} cm^{-1}. The extinction coefficient was calculated from a stock solution of TDH whose concentration was determined by amino acid analysis, performed at the University of Missouri Agricultural Experiment Station.

All common biochemicals and coupling enzymes were purchased from Sigma Chemical Co. Glucose-6-phosphate dehydrogenase was dialyzed against several liters of 100 mM K^+ HEPES at pH 8.0 before use. [2-^{2}H]Malate was prepared by the reduction of OAA by NaB^2H_4 (98 atom % deuterium, Aldrich Chemical Co.) and was used as the racemate. [2-^{3}H]-Malate was prepared as described before (Tipton, 1993) and had a specific activity of 5.9 μCi/μmol. The concentration of D-malate in the racemic solution of isotopically labeled malate and the concentration of stock solutions of unlabeled D-malate were calibrated by enzymatic end point assay with TDH. The concentration of free malate in solution was

† Supported by NIH Grant GM46836.

* Author to whom correspondence should be addressed. Telephone: (573) 882-7968. Fax: (573) 884-4812. E-mail: muccgw.bctipton@ssgate.missouri.edu.

⊗ Abstract published in *Advance ACS Abstracts,* February 15, 1996.

[1] Abbreviations: TDH, tartrate dehydrogenase; HEPES, *N*-(2-hydroxyethyl)piperazine-*N*′-2-ethanesulfonic acid; DTT, dithiothreitol; OAA, oxaloacetic acid.

0006-2960/96/0435-3108$12.00/0

calculated using a value of 173.8 M^{-1} for the Mn−malate association constant (Martell & Smith, 1977).

Transient-state kinetic studies were conducted using a KinTek SF-2000 stopped-flow spectrophotometer/spectrofluorimeter with a 2.6 cm long observation cell. A circulating water bath was used to maintain the temperature of the mixing block and the chamber which held the reactant syringes at 5 °C. The dead time of the instrument at 5 °C was determined to be 6 ms by monitoring the oxidation of glycyltryptophan by *N*-bromosuccinimide (Peterman, 1979). All time courses shown here represent the averaging of at least seven individual traces. The progress of the catalytic reaction was determined from the increase in absorbance at 340 nm due to formation of NADH ($\epsilon = 6220\ M^{-1}\ cm^{-1}$). Equilibrium titrations of NADH with TDH indicated that the extinction coefficient of enzyme-bound NADH is the same as that of the free species. Binding of the inhibitor tartronate was monitored by following the quenching of the intrinsic fluorescence of TDH which was associated with binding. The excitation wavelength used was 290 nm; emitted light which passed through a 10 nm band width filter centered at 340 nm was detected. The dissociation of NADH from Mn·TDH·NADH was detected by fluorescence resonance energy transfer from TDH to NADH; the sample was excited at 290 nm and emitted light which passed through a 10 nm band width filter centered at 450 nm was detected. Reaction conditions for each experiment are described in the figure legends. The data were analyzed by simulation of the time courses using the KINSIM program (Barshop et al., 1983), modified to run on a Macintosh computer by D. Wachsstock at Johns Hopkins University, and by nonlinear least-squares fitting of the time courses using the program FITSIM (Zimmerle & Frieden, 1989), as modified by the F. Raushel group at Texas A&M to run on a Silicon Graphics workstation.

Deuterium kinetic isotope effects were measured by direct comparison, and the tritium isotope effect was measured by an internal competition experiment. These experiments were conducted at 5 °C. In the direct comparison experiments, the reactions were carried out in 100 mM K^+ HEPES (pH 8.0) containing 0.6 mM NAD^+, 0.4 mM $Mn(OAc)_2$, 1 mM DTT, and either unlabeled or [2-^{2}H]malate, varying between 50 and 500 μM. The reaction solutions were mixed with enzyme in the stopped-flow instrument, and the reaction was followed for 1 s, by which time the steady-state velocity had been achieved. The velocity data were fitted to eq 1, in which $E_{V/K}$ is $^D(V/K) - 1$, E_V is $^DV - 1$, and F_i is the fractional enrichment of the deuterium in the D-malate.

$$v = \frac{VA}{K(1 + F_i E_{V/K}) + A(1 + F_i E_V)} \quad (1)$$

The internal competition experiments were conducted in solutions containing 0.4 mM $Mn(OAc)_2$ and 1 mM DTT in 100 mM K^+ HEPES at pH 8.0. Low-conversion samples contained 30 μM NAD^+ and 220 μM [2-^{3}H]-D-malate and were allowed to proceed until all of the NAD^+ had been utilized. The high-conversion samples contained 30 μM [2-^{3}H]-D-malate and 0.6 mM NAD^+ and were allowed to proceed until all of the D-malate had been utilized. After the reaction end point had been reached, each solution was immediately loaded onto a 1 mL column of benzyl-DEAE cellulose equilibrated in 10 mM potassium phosphate at pH 8.2. Unreacted D-malate was eluted with 15 mL of 10 mM potassium phosphate (pH 8.2), and the NADH was eluted with 9 mL of 100 mM potassium phosphate (pH 8.2). The eluant was collected directly into scintillation vials, and 9 mL of Scintiverse BD was added to each vial prior to counting. The value of $^T(V/K)$ was calculated according to eq 2, where R_p is the specific activity of the NADH formed in the low-conversion samples, R_o is the specific activity of the D-malate, and f is the fractional conversion of D-malate to products in the low-conversion samples.

$$^t(V/K) = \frac{\log(1-f)}{\log[1-f(R_p/R_o)]} \quad (2)$$

The value of R_o was determined from the specific activity of the NADH formed in the high-conversion samples.

The dissociation constant of NADH from the Mn·TDH complex was determined from inhibition studies of the forward reaction conducted at 5 °C using a Hewlett-Packard 8452A diode array spectrophotometer, with a water-jacketed cuvette holder connected to a circulating water bath. Reactions were conducted in solutions containing 2 mM $Mn(OAc)_2$ and 1 mM D-malate in 100 mM K^+ HEPES, pH 8.0 containing 1 mM DTT. The concentration of NAD^+ was varied between 50 and 540 μM; NADH was varied between 0 and 200 μM. The data were fit to eq 3 which describes competitive inhibition.

$$v = \frac{V_{max}A}{K_m(1 + I/K_i) + A} \quad (3)$$

The TDH-catalyzed partitioning of OAA between pyruvate and D-malate was determined using a fixed time assay in which pyruvate and OAA were determined by enzymatic end point assays. The partitioning was carried out in a total volume of 2.5 mL buffered at pH 8.0 with 100 mM HEPES; the solution contained 0.15 mM NADH, 0.4 mM $Mn(OAc)_2$, 0.6 mM glucose-6-phosphate, 0.5 mM OAA, 1 mM DTT, and 10 units of glucose-6-phosphate dehydrogenase. The glucose-6-phosphate/glucose-6-phosphate dehydrogenase couple served to regenerate NADH from any NAD^+ that was formed by the TDH-catalyzed reduction of OAA to D-malate, which served to make the TDH-catalyzed reaction irreversible. The solution was placed in a water bath at 5 °C and allowed to reach thermal equilibrium. An aliquot was removed for the determination of the exact concentration of OAA in the solution by end point assay with malate dehydrogenase. The partitioning reaction was initiated by the addition of 3.3 μM TDH. The reaction was allowed to proceed for 5 min at 5 °C and was quenched by the addition of 100 μL of $CHCl_3$, followed by vigorous vortexing for 1 min. Precipitated protein was removed by centrifugation, the concentration of OAA remaining in solution was determined by end point assay with malate dehydrogenase, and the concentration of pyruvate which had been generated was determined by end point assay with lactate dehydrogenase. Reaction blanks in which TDH was omitted were performed to determine the extent of nonenzymatic OAA decarboxylation which occurred during the course of the experiment.

RESULTS

Transient-State Kinetics. The time course for the TDH-catalyzed oxidative decarboxylation of D-malate is illustrated

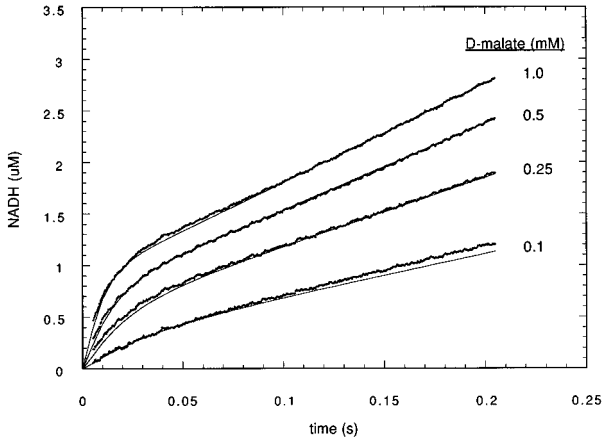

FIGURE 1: Time courses for the TDH-catalyzed oxidative decarboxylation of D-malate at 5 °C. Reaction conditions after mixing were 5 μM TDH, 0.4 mM $Mn(OAc)_2$, 1.5 mM NAD^+, and 1 mM DTT in 100 mM K^+ HEPES (pH 8.0). The solid lines for the time courses were calculated with FITSIM using the kinetic model shown in Scheme 1 as described in the text.

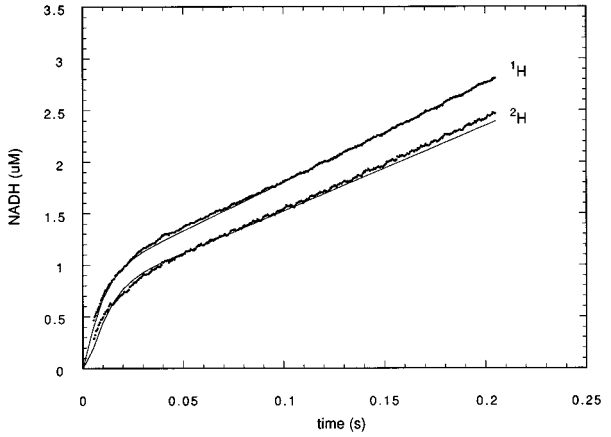

FIGURE 2: Time courses for the oxidation of 1 mM unlabeled and deuterated D-malate. Reaction conditions were identical to those described in the legend of Figure 1. The solid lines are the outcome of the simulation of the time courses using the values for the microscopic rate constants given in Table 1, except that k_5 and k_6 have been adjusted to account for an intrinsic isotope effect of 5.5 and an equilibrium isotope effect of 1.18.

in Figure 1. The K_m for D-malate is 80 μM, so these data span the range from approximately K_m levels of substrate up to saturation. A burst in product formation is evident; this burst disappears as the reaction temperature is raised (data not shown). All of the time courses at 5 °C were described well by the equation for a single exponential burst followed by a steady-state rate. The deuterium isotope effect on the reaction under saturating conditions is illustrated in Figure 2.

The rate constant for dissociation of NADH from TDH was measured directly by dilution of a solution of Mn·TDH·NADH into buffer (Figure 3). The fluorescence signal which arises from resonance energy transfer from the protein to the bound nucleotide decayed exponentially with a rate constant of 23.4 ± 0.2 s^{-1}. The dissociation constant for NADH from the enzyme was determined from steady-state kinetic inhibition experiments. NADH is a competitive inhibitor versus NAD^+; under the experimental conditions used here, K_i was 22 ± 3 μM. At 25 °C, the value for K_i for NADH determined from steady-state inhibition data is 32 μM (Tipton & Peisach, 1990) and the value determined from equilibrium fluoresence titrations is 28 ± 2 μM (data

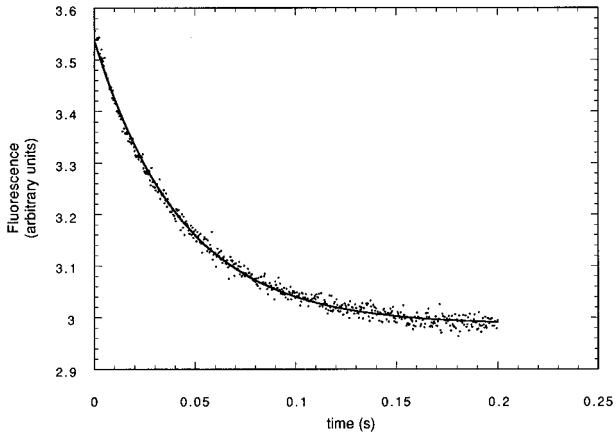

FIGURE 3: Dissociation of NADH from Mn·TDH·NADH at 5 °C. The sample was excited at 290 nm, and the emission at 350 nm was monitored. One syringe contained 0.4 μM TDH, 8 μM NADH, 0.4 mM $Mn(OAc)_2$, and 1 mM DTT in 100 mM K^+ HEPES; the other syringe contained buffer, $Mn(OAc)_2$, and DTT. The line is the fit of the data to a single exponential with a rate constant of 23.4 ± 0.2 s^{-1}.

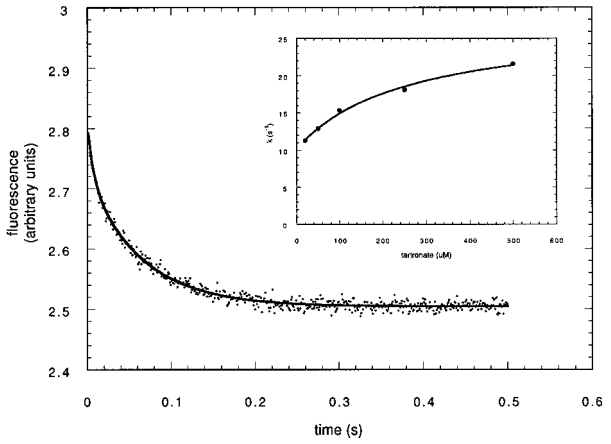

FIGURE 4: Binding of tartronate to Mn·TDH·NAD^+ at 25 °C, detected by the change in the protein fluorescence. The sample was excited at 290 nm, and the emission at 340 nm was monitored. The conditions after mixing were 5 μM TDH, 0.4 mM $Mn(OAc)_2$, 0.6 mM NAD^+, and 1 mM DTT in 100 mM K^+ HEPES (pH 8.0). As discussed in the text, the data were fitted to a double exponential, although the rate constant for the rapid phase of the reaction did not vary with tartronate concentration. The inset is tartronate concentration dependence of the rate constant describing the slow phase of the binding reaction. The data were fitted to eq 4 given in the text.

not shown). The rate constant for association of NADH with the enzyme at 5 °C can be calculated to be 1.05 × 10^6 M^{-1} s^{-1} from the relationship $K_D = k_{off}/k_{on}$.

Tartronate Binding. Binding of the inhibitor tartronate to the Mn·TDH·NAD^+ complex was examined by stopped-flow spectrofluorimetry. It was observed that tartronate binding induced a quenching of the protein's intrinsic fluorescence, and this signal could be used to monitor binding. A typical time course for tartronate binding is shown in Figure 4. The data fit a single exponential decay fairly well, but fit better to a double exponential. However, the value of one of the rate constants was invariant with tartronate concentration, at about 120 s^{-1}. The significance, if any, of this parameter is not clear at present. The other rate constant showed a hyperbolic dependence on tartronate concentration (Figure 4, inset). These data were fitted to eq 4, which describes a two-step binding mechanism in

Scheme 1

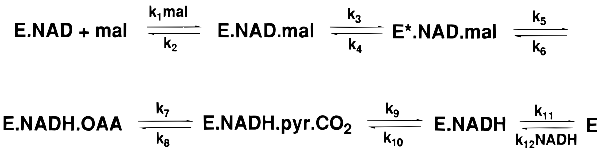

which the first step is in rapid equilibrium (Johnson, 1992).

$$k_{\rm obs} = \frac{K_1 k_2[\mathrm{S}]}{K_1[\mathrm{S}] + 1} + k_{-2} \qquad (4)$$

From this analysis, values of K_1, k_2, and k_{-2} were determined to be 0.004 ± 0.001 μM^{-1}, 17 ± 2 s^{-1}, and 10.2 ± 0.6 s^{-1}, respectively. The dissociation constant for tartronate is given by k_{-2}/K_1k_2; the value calculated in this way is 150 μM, which is in fair agreement with the value of 90 ± 4 μM, which was determined from equilibrium fluorescence titrations (data not shown).

Isotope Effect Determinations. Under steady-state conditions, the deuterium isotope effects were found to be 1.4 ± 0.2 for $^{\rm D}(V/K)$ and 1.2 ± 0.1 for $^{\rm D}V$. The tritium isotope effect, $^{\rm T}(V/K)$, was 1.86 ± 0.05.

OAA Partitioning. The TDH-catalyzed partitioning of exogenously added OAA between pyruvate and D-malate was determined by directly measuring the amount of pyruvate formed and by determining the amount of D-malate formed from the difference between the amount of OAA that was utilized and the amount of pyruvate that was formed. Control experiments showed that nonenzymatic decarboxylation accounted for about 15% of the pyruvate that was found in the partitioning experiments. After the data were corrected for nonenzymatic pyruvate formation, the ratio of pyruvate formed to D-malate formed was determined to be 0.15 ± 0.02. This result differs considerably from the value of 3.7 which was reported earlier (Tipton, 1993). In retrospect, it seems apparent that the experimental design used earlier was flawed, in that the pyruvate that was produced was coupled off, but formation of D-malate was reversible under the experimental conditions, with the net result that the reaction was pulled in the direction of pyruvate formation. In the present work, the formation of D-malate was made irreversible by prevention of the accumulation of NAD$^+$ using the glucose-6-phosphate/glucose-6-phosphate dehydrogenase couple. Reversal of OAA decarboxylation was considered to be negligible since the $K_{\rm m}$'s for pyruvate and CO_2 are approximately 5 and 12 mM, respectively. The intrinsic isotope effect on hydride transfer can be determined from the partition ratio and the values of $^{\rm D}(V/K)$ and $^{\rm T}(V/K)$ as described earlier (Tipton, 1993; Grissom & Cleland, 1985). This analysis yielded a value for $^{\rm D}k$ of 5.5.

Data Analysis. The time courses for the oxidative decarboxylation of D-malate shown in Figure 1 were fitted to the kinetic model in Scheme 1. Some simplifying assumptions were made in order to facilitate the analysis. First, it was assumed that the rates of release of pyruvate and CO_2 were not kinetically distinct steps. It was also assumed that pyruvate and CO_2 release, k_9, was not significantly rate-limiting and that rebinding occurred at a negligible rate, that is k_{10} is 0. Although there is no direct evidence that pyruvate and CO_2 release is not rate-limiting, TDH appears to have little affinity for either species, which suggests that it is reasonable to believe that their release is rapid. Pyruvate binding is undetectable in equilibrium fluorescence titration experiments; in the reverse reaction, the $K_{\rm m}$'s for pyruvate and CO_2 are approximately 5 and 12 mM, respectively (data not shown). The rate constant for reversal of OAA decarboxylation, k_8, was also set to zero, on the basis of the results of OAA partitioning studies (Tipton, 1993) and in accord with most analyses of enzyme-catalyzed oxidative decarboxylations (Hermes et al., 1982; Grissom & Cleland, 1985). The rate constant for NADH dissociation, k_{11}, was determined directly, and the rate constant for its association was calculated from the equilibrium dissociation constant and the rate constant for dissociation.

Table 1: Rate Constants for the TDH-Catalyzed Oxidative Decarboxylation of D-Malate[a]

rate constant	value	rate constant	value
k_1 (M^{-1} s^{-1})	(2.3 ± 0.1) × 10^6	k_2 (s^{-1})	10 400 ± 600
k_3 (s^{-1})	600 ± 30	k_4 (s^{-1})	27 ± 1
k_5 (s^{-1})	320	k_6 (s^{-1})	1000
k_7 (s^{-1})	11.2 ± 0.1	k_8 (s^{-1})	0
k_9 (s^{-1})	ND[b]	k_{10} (M^{-1} s^{-1})	0
k_{11} (s^{-1})	23	k_{12} (M^{-1} s^{-1})	1.05 × 10^6

[a] The rate constants were determined by fitting the data in Figure 1 to the kinetic mechanism shown in Scheme 1, using the program FITSIM. The rate constants k_1, k_2, k_3, k_4, and k_7 were allowd to vary, and the other rate constants were fixed at the values shown. The manner in which the other rate constants were determined is discussed in the text. [b] Not determined; for the purpose of fitting the time courses, k_9 was assigned a value of 1000 s^{-1}.

The other rate constants in the kinetic scheme were initially allowed to vary when the data in Figure 1 were analyzed with FITSIM. It became apparent, however, that, although the ratio of k_5 to k_6 was determined well by this analysis, the absolute magnitude of those rate constants was not determined well. In order to obtain a reasonable estimate of their magnitude, the isotope effect data shown in Figure 2 were examined. The time courses for oxidation of unlabeled and deuterated malate must be reproduced by the same set of rate constants, allowing only for differences in k_5 and k_6 arising from the intrinsic isotope effect of 5.5 on hydride transfer and an equilibrium isotope effect of 1.18 (Cook et al., 1980). The time courses were simulated with KINSIM using different values of k_5 and k_6, which were kept in the appropriate ratio determined from the FITSIM analysis. After a satisfactory fit to the time courses for both unlabeled and deuterated malate was obtained, the time courses shown in Figure 1 were reanalyzed, again allowing k_1, k_2, k_3, k_4, and k_7 to vary, but holding k_5 and k_6 constant at the values determined from the simulation. This iteration through FITSIM did not result in very significant changes in the values of the varied rate constants compared to their values when k_5 and k_6 were allowed to vary.

The rate constants derived from this analysis are given in Table 1. The errors shown are those from the FITSIM analysis of a single data set and indicate how sensitive the data are to the value of each rate constant. Analysis of another set of experimental data collected with another set of solutions yielded very similar values. As would be expected, the rate constants governing the rate-limiting steps are better defined than those governing steps which contribute little to the overall rate. With the variation in rate constants derived from analysis of different data sets taken into

account, the errors on the rate constants should be considered to be on the order of 10%.

DISCUSSION

The key to understanding the specificity of product formation in TDH-catalyzed reactions lies in determining whether the lower-energy pathway for each intermediate along the reaction pathway is dissociation from the active site or further chemical transformation. The (+)-tartrate reaction is distinct from the D-malate and *meso*-tartrate pathways because the β-keto acid formed in the former reaction, (3*R*)-oxaloglycolate, is released by the enzyme, whereas the β-keto acids formed from the other substrates remain bound at the active site. Similarly, the D-malate and *meso*-tartrate pathways diverge after decarboxylation of the β-keto acid intermediates, when pyruvate dissociates, but hydroxypyruvate remains bound and undergoes reduction by regaining the hydride that was transferred to NAD^+ in the first step in the reaction.

A description of the internal energetics of each pathway will reveal the energy differences which determine the fate of each intermediate. In this work, transient-state kinetics, in conjunction with isotope effect measurements, have been applied to derive a kinetic description of the D-malate reaction.

The data were interpreted within the framework of the kinetic mechanism shown in Scheme 1, and it is worthwhile examining the salient features of this model. First, the model encompasses only the binding of the last substrate, D-malate. It has been determined that TDH follows an ordered kinetic mechanism with Mn^{2+} binding first, followed by NAD^+ and D-malate (Tipton & Peisach, 1990). All of the pre-steady-state kinetic experiments were conducted by addition of D-malate to the already-formed Mn·TDH·NAD^+ complex.

Binding of D-malate is shown as a two-step process. This conforms to a mechanism by which steady-state kinetic isotope effects are often evaluated, which distinguishes between the collision complex formed by the addition of the last substrate and the Michaelis complex from which reaction occurs and gives rise to the internal portion of the forward commitment to catalysis (Cleland, 1982). In the case of TDH, there are several independent lines of evidence which suggest a physical basis for this step. Pulsed electron paramagnetic resonance studies of TDH active site complexes have shown that Mn^{2+} and the nicotinamide ring of NAD^+ or NADH approach each other upon the binding of oxalate, an inhibitor of the enzyme (Tipton & Peisach, 1991). Analysis of the kinetics of oxalate inhibition has led to the suggestion that the protein undergoes a conformation change upon oxalate binding, and it has been proposed that this conformation change is an integral part of the normal catalytic reaction, in which the formation of a closed complex serves to prevent premature dissociation of reaction intermediates (Beecher et al., 1994). Finally, the data shown in Figure 4 are consistent with binding of the last substrate, or an analog of it such as tartronate, being accompanied by an enzyme conformation change. The fact that the intrinsic fluorescence of the protein changes upon tartronate binding argues for some degree of motion at the active site. Furthermore, the hyperbolic dependence of the observed rate constant for binding on tartronate concentration is consistent with a two-step binding mechanism (Johnson, 1992). Unfortunately, it was not possible to examine D-malate binding directly because of the difficulty in distinguishing changes in the protein fluorescence due to conformation changes from those due to formation of NADH via catalysis.

The next steps encompass the chemical steps, in which hydride transfer is presumed to precede decarboxylation. This mechanism is well-established for enzymes which catalyze metal-dependent oxidative decarboxylations (Hermes et al., 1982; Grissom & Cleland, 1988). Although multiple isotope effect measurements have not been applied to the D-malate reaction to prove the intermediacy of OAA, the fact that TDH catalyzes the partitioning of OAA between D-malate and pyruvate argues strongly that OAA is a discrete intermediate in the normal catalytic reaction. The overall reaction is reversible; however, under initial velocity conditions in the forward direction, the recarboxylation of pyruvate (shown as k_8 in Scheme 1) occurs at a negligible rate (Tipton, 1993).

Product release is considered to occur in two steps. Steady-state kinetic studies have shown that NADH dissociates after pyruvate and CO_2, but the order in which the latter two species dissociate is not clear. Thus, their dissociation has been conflated into a single kinetic step. Unfortunately, it has not been possible to assign a value to the rate constant for pyruvate and CO_2 release, and in the present analysis, it was assumed that the rate constant was high enough that it was not rate-limiting. This assumption seems borne out by the good agreement between experimental and calculated values for the steady-state kinetic parameters, as discussed below. The rate constant for release of NADH was determined directly and found to be 23 s^{-1}. It therefore contributes to the overall rate of the reaction, and the fact that NADH release is partially rate-limiting is reflected in the greater attenuation of the expression of ^Dk in ^DV than in $^D(V/K)$.

The reliability and consistency of the values for the rate constants shown in Table 1 can be examined by comparison of the experimentally measured isotope effects, the OAA partition ratio, and the steady-state kinetic parameters with the values for these parameters calculated from the microscopic rate constants (Table 2). The agreement between the experimentally determined parameters and the calculated ones is quite reasonable. The agreement between the observed value for V_{max} and the value calculated from the microscopic rate constants lends credence to the assumption used in the analysis that pyruvate and CO_2 release are not rate-limiting. It is also reassuring to find that the time course obtained with [^{2}H]malate could be simulated by changing only the rate constants governing the isotope-sensitive steps. In fact, this experiment was crucial for the analysis, because it was observed that the time courses shown in Figure 1 were relatively insensitive to the absolute magnitudes of the values for k_5 and k_6 but were quite sensitive to the ratio of k_5 to k_6. However, simulations of the time courses for oxidation of unlabeled malate and deuterated malate (Figure 2), which are subject to the strictures that rate constants for isotope-insensitive steps cannot change, and that ^Dk is 5.5, were sensitive to the magnitudes of k_5 and k_6 so that estimates of values of these parameters could be made.

Another check on the consistency of the calculated rate constants can be performed by comparison of the value of the dissociation constant for D-malate calculated from kinetic isotope effect data with that calculated from the microscopic rate constants. Klinman and Matthews (1985) have shown

Table 2: Comparison of Calculated and Experimentally Determined Reaction Parameters

parameter	expression[a]	experimental value	calculated value
(V/KE_t)	$\frac{k_1k_3k_5/k_2k_4}{1 + c_f + c_r}$	$0.017 \pm 0.001\ \mu M^{-1}\ s^{-1}$	$0.015\ \mu M^{-1}\ s^{-1}$
(V_{max}/E_t)	$\frac{k_3k_5/(k_3 + k_4)}{1 + c_{Vf} + c_r}$	$2.09 \pm 0.05\ s^{-1}$	$2.27\ s^{-1}$
$^D(V/K)$	$\frac{^Dk + c_f + c_r{}^DK_{eq}}{1 + c_f + c_r}$	1.4 ± 0.2	1.2
^DV	$\frac{^Dk + c_{Vf} + c_r{}^DK_{eq}}{1 + c_{Vf} + c_r}$	1.2 ± 0.1	1.2
$^T(V/K)$	$\frac{^Dk^{1.442} + c_f + c_r{}^DK_{eq}{}^{1.442}}{1 + c_f + c_r}$	1.8 ± 0.1	1.3
r	$\frac{1 + c_f}{c_r}$	0.15 ± 0.02	0.15

[a] The parameters in these expressions are defined as follows: $c_f = k_5/k_4(1 + k_3/k_2)$; $c_r = k_6/k_7(1 + k_8/k_9)$; $c_{Vf} = [k_5/(1 + k_4/k_3)](1/k_3 + 1/k_7 + k_8/k_7k_9 + 1/k_9 + 1/k_{11})$. A value of 5.5 was used for ^Dk.

that $^D(V/K)$ and ^DV are related to K_m and K_d by eq 5, where K_d is given by $k_2k_4/[k_1(k_3 + k_4)]$.

$$\frac{^DV - 1}{^D(V/K) - 1} = \frac{K_m}{K_d} \quad (5)$$

The K_m for D-malate at 5 °C is 83 μM, which, in conjunction with the values of ^DV and $^D(V/K)$ determined in this study, leads to a calculated value of 170 μM for K_d. Using the values for the relevant microscopic rate constants in Table 1, the calculated value for K_d is 190 μM.

It is apparent that hydride transfer is not very rate-limiting in the oxidation of D-malate. The isomerization of the E·NAD·malate complex and the decarboxylation of E·NADH·OAA are both kinetically significant steps which contribute to the forward and reverse commitment factors and attenuate the expression of ^Dk. The smallest rate constant is that for decarboxylation of OAA. It is possible that this is a consequence of the fact that since the "natural" substrate of TDH is (+)-tartrate, which does not undergo decarboxylation, there is no selective pressure acting to increase the efficiency of decarboxylation. However, there are reasons to doubt this explanation, since several enzymes which catalyze analogous reactions exhibit rate-limiting decarboxylation. On the basis of sequence homology, TDH appears to be closely related to the other metal-dependent decarboxylating dehydrogenases isopropylmalate dehydrogenase and isocitrate dehydrogenase (Tipton & Beecher, 1994). In the case of pig heart isocitrate dehydrogenase, decarboxylation is largely rate-limiting at low pH (Grissom & Cleland, 1988). Malic enzyme, to which TDH is not related, but which catalyzes the oxidative decarboxylation of L-malate, has been observed to proceed with rate-limiting decarboxyation of OAA (Hermes et al., 1982; Weiss et al., 1991). Thus, slow decarboxylation may be an intrinsic feature of these enzymatic reactions. Another explanation for the results obtained in this study, which cannot be critically assessed with the available data, is that decarboxylation is rapid and kinetically indistinguishable from a slow step following it. This explanation has the appealing feature that the slow step could be assigned to the reopening of the active site to allow product dissociation. Measurements of $^{13}(V/K)$ will be useful for examination of this proposal.

Tight binding of the intermediate OAA is presumably necessary to prevent its premature dissociation. The D-malate and (+)-tartrate reactions diverge at the stage of the Mn·TDH·NADH·β-keto acid complex, where oxaloglycolate from (+)-tartrate is released and OAA from D-malate remains bound. It was earlier shown that the rate of release of OAA from this complex could be estimated by means of a thermodynamic box relating formation of Mn·TDH·NADH·OAA from D-malate and NAD^+ via the normal catalytic reaction and from exogenously added OAA and NADH (Tipton, 1993; Cleland, 1990). This calculation requires an estimate of the internal equilibrium constant for hydride transfer, which was previously assumed to be equal to 1; this estimate can now be revised to a value of 0.3, on the basis of the data in Table 1. The resulting calculated rate constant for the release of OAA from the Mn·TDH·NADH·OAA complex is $2 \times 10^{-4}\ s^{-1}$. Therefore, decarboxylation of OAA is 6 kcal/mol more favorable than release of OAA from this complex. It is evident that, although the TDH reaction cycle can be terminated at this stage with some substrates by release of the carbon acid product, in the case of D-malate, it is firmly committed to further chemical transformation. Presumably, the high energetic barrier to release arises because the enzyme complex is still in a closed form. This raises the interesting, and as yet unanswered, question of what determines when the complex opens to release the products.

REFERENCES

Barshop, B. A., Wrenn, R. F., & Frieden, C. (1983) *Anal. Biochem. 130*, 134−145.

Beecher, B. S., Koder, R. L., & Tipton, P. A. (1994) *Arch. Biochem. Biophys. 315*, 255−261.

Cleland, W. W. (1982) *Crit. Rev. Biochem. 13*, 385−428.

Cleland, W. W. (1990) *Biochemistry 29*, 3194−3197.

Cook, P. F., Blanchard, J. S., & Cleland, W. W. (1980) *Biochemistry 19*, 4853−4858.

Grissom, C. B., & Cleland, W. W. (1985) *Biochemistry 24*, 944−948.

Grissom, C. B., & Cleland, W. W. (1988) *Biochemistry 27*, 2934−2943.

Hermes, J. D., Roeske, C. A., O'Leary, M. H., & Cleland, W. W. (1982) *Biochemistry 21*, 5106−5114.
Johnson, K. A. (1992) *The Enzymes*, 3rd ed., pp 1−61, Academic Press, New York.
Klinman, J. P., & Matthews, R. G. (1985) *J. Am. Chem. Soc. 107*, 1058−1060.
Martell, A. E., & Smith, R. M. (1977) *Critical Stability Constants*, Vol. 3, Plenum Press, New York.
Peterman, B. F. (1979) *Anal. Biochem. 93*, 442−444.
Tipton, P. A. (1993) *Biochemistry 32*, 2822−2827.
Tipton, P. A., & Peisach, J. (1990) *Biochemistry 29*, 1749−1756.
Tipton, P. A., & Peisach, J. (1991) *Biochemistry 30*, 739−744.
Tipton, P. A., & Beecher, B. S. (1994) *Arch. Biochem. Biophys. 313*, 15−21.
Weiss, P. M., Gavva, S. R., Urbauer, J. L., Harris, B. G., Cleland, W. W., & Cook, P. F. (1991) *Biochemistry 30*, 5755−5763.
Zimmerle, C. T., & Frieden, C. (1989) *Biochem. J. 258*, 381−387.

BI9518454